Editors' Suggestion | Featured in Physics

Double-Free-Layer Magnetic Tunnel Junctions for Probabilistic Bits

Kerem Y. Camsari,[1,*] Mustafa Mert Torunbalci,[2] William A. Borders,[3] Hideo Ohno,[3,4,5,6,7] and Shunsuke Fukami[3,4,5,6,7]

[1] *Department of Electrical and Computer Engineering, University of California, Santa Barbara, California 93106, USA*

[2] *Birck Nanotechnology Center, Purdue University, West Lafayette, Indiana 47907 USA*

[3] *Laboratory for Nanoelectronics and Spintronics, Research Institute of Electrical Communication, Tohoku University, Japan*

[4] *Center for Spintronics Research Network, Tohoku University, Japan*

[5] *Center for Science and Innovation in Spintronics, Tohoku University, Japan*

[6] *WPI Advanced Institute for Materials Research, Tohoku University, Japan*

[7] *Center for Innovative Integrated Electronic Systems, Tohoku University, Japan*

(Received 13 December 2020; revised 3 March 2021; accepted 25 March 2021; published 29 April 2021)

Naturally random devices that exploit ambient thermal noise have recently attracted attention as hardware primitives for accelerating probabilistic computing applications. One such approach is to use a low barrier nanomagnet as the free layer of a magnetic tunnel junction (MTJ), the magnetic fluctuations of which are converted to resistance fluctuations in the presence of a stable fixed layer. Here, we propose and theoretically analyze a MTJ with no fixed layers but two free layers that are circularly shaped disk magnets. We use an experimentally benchmarked model that accounts for finite-temperature magnetization dynamics, bias-dependent charge, and spin-polarized currents as well as the dipolar coupling between the free layers. We obtain analytical results for statistical averages of fluctuations that are in good agreement with the numerical model. We find that the free layers with low diameters fluctuate to randomize the resistance of the MTJ in an approximately bias-independent manner. We show how such MTJs can be used to build a binary stochastic neuron (or a p-bit) in hardware. Unlike earlier stochastic MTJs that need to operate at a specific bias point to produce random fluctuations, the proposed design can be random for a wide range of bias values, independent of spin-transfer-torque pinning. Moreover, in the absence of a carefully optimized stabled fixed layer, the symmetric double-free-layer stack can be manufactured using present-day magnetoresistive random-access memory (MRAM) technology by minimal changes to the fabrication process. Such devices can be used as hardware accelerators in energy-efficient computing schemes that require a large throughput of tunably random bits.

DOI: 10.1103/PhysRevApplied.15.044049

I. INTRODUCTION

Intrinsic randomness in nanodevices can be harnessed to do useful computational tasks, especially when the natural physics of a device map to a useful functionality, a principle sometimes expressed as "let physics do the computing" [1]. One such example is the physics of low-barrier magnets, which can produce random fluctuations in magnetization that can be turned into fluctuations in resistances in magnetic tunnel junctions (MTJs). Stochastic MTJs (SMTJs) and the stochastic behavior of MTJs have attracted a lot of recent attention, both theoretically and experimentally [2–12,12–21]. It has been observed that even with the relatively modest tunneling magnetoresistance of present-day MTJs, where the parallel to antiparallel resistance ratios are small, fluctuations in resistances can be converted to electrical fluctuations that can be sensed by inverters or amplifiers [14,22]. Such devices can be useful as compact energy-efficient tunable true random number generators that can be interconnected to accelerate a wide range of computational tasks such as sampling and optimization [23].

Both theory and available experimental data suggest that when SMTJs are designed out of perpendicular easy-axis MTJs (PMTJs), where both the fixed and the free layer have perpendicular anisotropy, the fluctuations tend to be slow, since even at the zero-barrier limit $E/k_BT \to 0$ (where E is the energy barrier of the magnet, k_B is the Boltzmann constant, and T is the temperature) the fluctuations (τ) are of the order of $\tau^{-1} \approx \alpha\gamma H_{\text{th}}$ (where γ is the

*camsari@ece.ucsb.edu

gyromagnetic ratio of the electron, α is the damping coefficient, and H_{th} is an effective thermal noise field, given by $H_{\text{th}} = k_B T/M_s \mathcal{V}$, $M_s \mathcal{V}$ being the total magnetic moment) [24]. Even for a small magnet—for example, with half a million spins—τ^{-1} is limited to frequencies around 1.5–15 MHz for $\alpha = 0.01$–0.1. An alternative is to use circular-disk magnets with no intrinsic anisotropy, since by virtue of their large demagnetizing field, these magnets tend to produce much faster fluctuations [22,25] with a precessional mechanism that has been theoretically analyzed [26–28] and recently observed in experiment [20,29]. All focus on SMTJs, whether with in-plane or perpendicular easy-axis magnets, however, has been on magnetic stacks, where there is a stable fixed layer and an unstable free layer that fluctuates in the presence of thermal noise. The current standard in spin-transfer-torque magnetoresistive random access memory (STT MRAM) technology is to use PMTJs [30] and switching to such in-plane easy-axis magnets with at least one stable fixed layer to get fast fluctuations is challenging from an industry standpoint, especially for miniaturized MTJs down to a few tens of nanometers, where techniques to fabricate fixed layers have not been established.

In this paper, we propose and evaluate the possibility of using a *double-free-layer* MTJ where both layers are designed as circular in-plane easy-axis magnets. Such a configuration can easily be achieved by starting from a typical STT MRAM material-stack structure comprised of Co-Fe-B/MgO/Co-Fe-B MTJs by making both the free- and fixed-layer magnets thicker such that their easy-axis orients in the plane of the magnet (Fig. 1). In the rest of this paper, we analyze the behavior of this double-free-layer MTJ device. One advantage of this device comes from its simplicity: it is a completely symmetric device with two free layers that are in an in-plane configuration in equilibrium and this does not require a highly optimized magnetic stack design as it is based on the same Co-Fe-B/MgO/Co-Fe-B structure of standard PMTJs. Another key feature of this device is its bias independence over a wide range of voltages, which can be useful for designing devices to be used in probabilistic computing applications where a large throughput of tunable random bit streams are needed. We note that double-free-layer structures similar to those shown in Fig. 1 have been discussed in the context of spin-torque nano-oscillators (see, for example, Refs. [31–35]); however, our focus in this paper is on fully circular magnets with no intrinsic anisotropy that are in the superparamagnetic regime.

The rest of the paper is organized as follows. In Sec. II, we develop a model to describe the dipolar interaction between the layers, starting from Maxwell's equations in the magnetostatics regime. In Sec. III, we describe the finite-temperature coupled-macrospin model that describes the magnetization dynamics. In Sec. IV, we analyze the zero-bias behavior of the double-free-layer MTJ with analytical benchmarks that are obtained from equilibrium statistical mechanics. In Sec. V, we describe the fully voltage-dependent model that considers bias-dependent spin-polarized currents that influence the free layers. Finally, in Sec. VI, we show how the proposed device can be combined with modern transistors in a 1 transistor (1T)-1MTJ circuit topology to deliver tunable randomness with fast fluctuations.

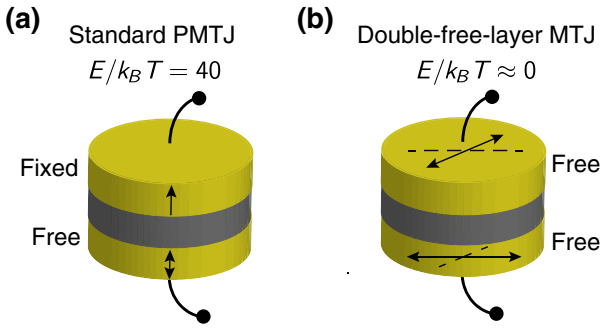

FIG. 1. The proposed device. (a) The standard MTJ of the MRAM technology using perpendicular easy-axis MTJs (PMTJs) with fixed and free layers. (b) We consider an MTJ with two free layers and no fixed layer. The magnetization of the free layers fluctuates in the plane in the presence of thermal noise that is turned into resistance fluctuations through tunneling magnetoresistance (TMR). One way to build the proposed device is to start from the standard PMA-MTJs and make both the free and the fixed layers thicker so that their magnetizations fall into the plane. We note that the PMTJ stack sketch shown here is for illustrative purposes and that industrial PMTJ stacks have many more additional layers that account for canceling dipolar fields, ensuring fixed-layer stability and other effects.

II. MAGNETOSTATICS

In the absence of any external magnetic field and intrinsic anisotropies, the energy of the two-magnet system is fully specified by magnetostatics and is given by [36]

$$E = -2\pi M_s^2 \mathcal{V} \left(\sum_{i=1}^{2} \hat{m}_i^T N_{ii} \hat{m}_i + \sum_{\substack{i,j \\ i \neq j}}^{2} \hat{m}_i^T D_{ij} \hat{m}_j \right), \quad (1)$$

where M_s is the magnetic moment per volume, $\mathcal{V}$ is the volume, the $\hat{m}_i$ are the three-component magnetization vectors, and N_{ii} and D_{ij} are the demagnetization and the dipolar tensors, respectively (we adopt cgs units for magnetic models throughout). We implicitly assume the volume and the M_s to be the same for both magnets, which is true for all cases considered in this paper. We adopt a macrospin approach where the chosen volume corresponds to the volume of the magnet and the $\hat{m}_i$ are described as three-component vectors. We numerically solve for **D** and

N that are in general position dependent but we average them within the volume of the target magnet to reduce these to single numbers for a given geometry.

Starting from the magnetostatics conditions where $\vec{\nabla} \times \vec{H} = 0$, we can define a magnetic potential Φ such that $-\nabla\Phi = \vec{H}$ and since $\vec{\nabla} \cdot \vec{B} = 0$ and $\vec{B} = (\vec{H} + 4\pi\vec{M})$ always hold, we obtain $\nabla^2\Phi = 4\pi\,\vec{\nabla} \cdot \vec{M}$, which is mathematically equivalent to the Poisson equation of electrostatics. To solve this equation, we first introduce a Green's function, $G(\vec{r}, \vec{r'})$, defined as the potential at $\vec{r}$ due to a "unit" charge at source $\vec{r'}$. G can be readily identified from the definition of the Dirac delta function [37], $\nabla^2(-1/|\vec{r} - \vec{r'}|) \equiv 4\pi\delta(\vec{r} - \vec{r'})$. Once this Green's function is known, using the linearity of the potential [38], we can write the general solution for the magnetic potential as

$$\Phi(\vec{r}) = \int d\vec{r'} G(r, \vec{r'}) \rho_M(r'), \tag{2}$$

where we have defined a magnetic source density, $\rho_M(r') = 4\pi\vec{\nabla} \cdot \vec{M}$, which is only nonzero at the boundaries of the magnetic volume, assuming a uniformly magnetized body. The solution to the magnetic potential at position $\vec{r}$ then becomes

$$\Phi(\vec{r}) = \int_{\mathcal{V}} \frac{-\vec{\nabla} \cdot \vec{M}}{|\vec{r} - \vec{r'}|} d\Omega, \tag{3}$$

where $\mathcal{V}$ is the volume of the source magnet. Now let us consider the specific case shown in Fig. 2(a), where we have a cylindrical in-plane magnet, $\hat{M} = M_s\hat{x}$. The magnetic source density can be expressed as $-\vec{\nabla} \cdot \vec{M} = M_s\delta(R - r')\cos\phi$, since the magnetization abruptly becomes zero right outside the magnetic boundary. This allows us to write the magnetic potential as follows:

$$\Phi(\vec{r}) = \int_{-\delta}^{\delta}\int_{0}^{2\pi} \frac{d\phi\, dz' \cos(\phi) M_s R}{\sqrt{(x - R\cos\phi)^2 + (x - R\sin\phi)^2 + (z - z')^2}}, \tag{4}$$

where we introduce $\delta = t/2$, t being the thickness of the magnetic layer (source). We do not find a closed-form solution of this integral, though it can be partly integrated just along z' after taking derivatives of Φ to obtain field expressions. These are not necessarily informative, so we do not repeat them here but we use these partial integrals to ease the numerical integration of Eq. (4) (for another treatment, see, e.g., [39]). Figure 2(b) shows a typical position-dependent vector plot of this numerical integration. In Fig. 2(c), we show typical results where the field strength increases for magnets with lower diameters, also observed in experiments with perpendicular MTJs [40] [also, see the inset in Fig. 4(a) for averaged out $D_{xx} = D_0$ values]. This correspondence between PMTJs and the double-free-layer system considered here can be seen from the properties of the dipolar tensor, i.e., tr[**D**] = 0 [41,42].

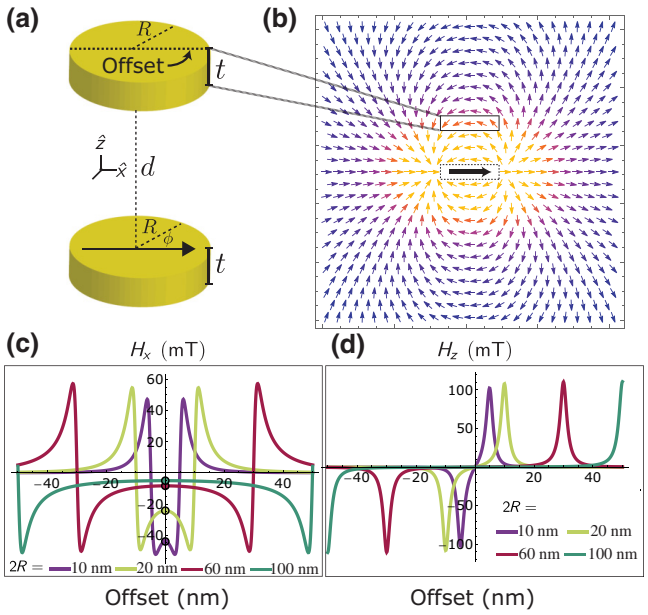

FIG. 2. The dipolar model. (a) The geometry and parameters in the calculation of dipolar fields between the two free layers. (b) An illustrative vector plot of the dipolar field due to the bottom layer (dashed box) at the $y = 0$ plane. (c) The dipolar field H_X due to a source magnet (bottom, $+x$ polarized) with varying diameters ($2R = 10, 20, 60, 100$ nm) with a film thickness of $t = 1$ nm at a distance $d = 1$ nm (typical MgO thickness in MTJs) measured from the top of the source magnet with $M_s = 800$ emu/cc ≈ 1 T. At zero offset (circled points), the fields can be analytically calculated from Eq. (5). (d) The z-directed fields along the offset direction. In our model, these fields average out to zero when summed over the target magnetic volume.

As mentioned earlier, our approach of calculating dipolar tensor components is by averaging the field over the target magnetic body; for example, to compute D_{xx}, we first compute H_X over the target magnet volume when the source is magnetized along $+x$ and take an average of this field to obtain a single value for D_{xx}. Equation (4) can easily be integrated on the cylindrical axis ($x = 0, y = 0$) after taking the derivative $H_Z = -\partial\Phi/\partial z$ and this results in

$$H_Z = \pi M_s \left(\frac{z - \delta}{\sqrt{R^2 + (z - \delta)^2}} - \frac{z + \delta}{\sqrt{R^2 + (z + \delta)^2}} \right). \tag{5}$$

Figure 2(c) shows the application of this formula at zero offset, which is defined as the dashed line in Fig. 2(a) that passes along the $y = 0$ line, and this result matches the numerical integration. It might be tempting to use Eq. (5) to approximate the dipolar tensor coefficients analytically to obtain a single number but we find that this tends to significantly differ from the value we obtain after averaging

over the volume, especially at larger diameters. With this method of calculating dipolar coefficients, we find that D_{xy}, D_{yx}, D_{zx}, and D_{zy} all average to zero, which only leaves the diagonal components [see Fig. 2(d)]. Moreover, the cylindrical symmetry of the problem ensures that $D_{xx} = D_{yy} = D_0$ and from the symmetry of the dipolar tensor $D_{zz} = -2D_0$, leaving only one tensor coefficient to compute. Similarly, the diameter ($2R$) to thickness (t) ratios of all the magnets analyzed in this paper ensure that $t/R \ll 1$, and the demagnetization tensor always has one component, $N_{zz} \approx -1$, which is what we use in the rest of the paper.

III. MAGNETIZATION DYNAMICS

Next, we describe the coupled magnetization dynamics model that considers two coupled Landau-Lifshitz-Gilbert (LLG) equations at finite temperature [43–45]:

$$(1+\alpha^2)\frac{d\hat{m}_i}{dt} = -|\gamma|\hat{m}_i \times \vec{H}_i - \alpha|\gamma|(\hat{m}_i \times \hat{m}_i \times \vec{H}_i) + \frac{1}{qN}[\hat{m}_i \times \vec{I}_{S_i}(V) \times \hat{m}_i] + \left\{\frac{\alpha}{qN}[\hat{m}_i \times \vec{I}_{S_i}(V)]\right\}, \quad (6)$$

where α is the damping coefficient, γ is the gyromagnetic ratio of the electron, q is the electron charge, and i is the magnet index, $i \in \{1,2\}$. The effective field for each magnet is calculated according to Eq. (1), $H_i \equiv -\nabla_{\hat{m}} E/(M_s \mathcal{V})$ and $N = (M_s \mathcal{V})/\mu_B$, and μ_B is the Bohr magneton. The effective field H_i includes uncorrelated Gaussian noise ($H^n_{x,y,z}$) at each direction (x,y,z) with the following statistical properties: $\langle H^n(t)\rangle = 0$ and $\langle H^n(t)H^n(t')\rangle = D\delta(t-t')$, where $D = (2\alpha k_B T)/(\gamma M_s \mathcal{V})$. In our model, this set of equations is solved self-consistently with a transport model for the MTJ, which provides the bias-dependent spin-polarized current, $\vec{I}_S(V)$ at a given bias, which in turn depends on the instantaneous magnetizations, m_i (Fig. 3).

An important consideration when modeling circular-disk nanomagnets in the macrospin approximation is the formation of vortex states [46]. However, for the highly reduced diameters (≤ 100 nm) and thicknesses (≤ 1 nm) considered in this paper, both detailed micromagnetic simulations [47–49] and available experiments [50–52] indicate that the macrospin-modeling approach in the parameter ranges considered should be reasonably informative.

We solve the stochastic LLG equation using the transient-noise function of HSPICE. We benchmark this model extensively by comparing its time-dependent statistical behavior with respect to the Fokker-Planck equation [53] and also by comparing it against our own implementation that solves the stochastic LLG equation using the Stratonovitch convention [54].

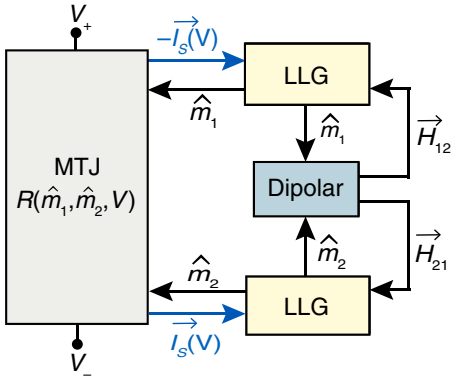

FIG. 3. The self-consistent model for the magnetization dynamics and transport. The coupled LLG equations provide instantaneous magnetizations to the MTJ model, which in turn produces a bias-dependent spin-polarized current, $\vec{I}_S(V)$ in the channel. $+\vec{I}_S(V)$ is incident to one ferromagnetic interface and $-\vec{I}_S(V)$ is incident to the other ferromagnetic interface. The dipolar model couples the two LLG solvers through fields that depend on instantaneous $\hat{m}_i$.

IV. ZERO-BIAS BEHAVIOR

It is instructive to analyze the zero-bias behavior ($V = 0 \rightarrow \vec{I}_S = 0$) of the two free layers before considering their interaction with spin-polarized currents. Starting from Eq. (1) and making use of the symmetry results described at the end of Sec. II, we can write

$$E = -4\pi M_s^2 \mathcal{V}\left[-\frac{(m_1^z)^2}{2} - \frac{(m_2^z)^2}{2} + (D_0)m_1^x m_2^x + (D_0)m_1^y m_2^y - (2D_0)m_1^z m_2^z\right]. \quad (7)$$

Since both free layers are low-barrier magnets that fluctuate in the presence of thermal noise, it is instructive to calculate the cosine of the average angle between the free layers ($\cos\theta_{1,2}$) at zero bias, as this determines the resistance of the MTJ. This average can be written down from the Boltzmann distribution (switching to spherical coordinates):

$$\langle\cos\theta_{1,2}\rangle = \frac{1}{Z}\int \hat{m}_1 \times \hat{m}_2 \exp\left[\frac{-E(\theta,\phi,\eta,\chi)}{k_B T}\right] d\theta d\phi d\eta d\chi, \quad (8)$$

where (θ,ϕ) and (η,χ) are spherical coordinate pairs for the two magnets and Z is a normalization constant that ensures that the total probability is 1. We cannot find a closed-form expression for this integral but we can make progress by approximations. Introducing $h_d \equiv 4\pi M_s^2 \mathcal{V}/k_B T$ and $d_0 = D_0 h_d$, we note that for typical parameters ($M_s = 800$ emu/cc and $2R = 10 - 100$ nm), $h_d \gg 1$, indicating that both magnets always roughly

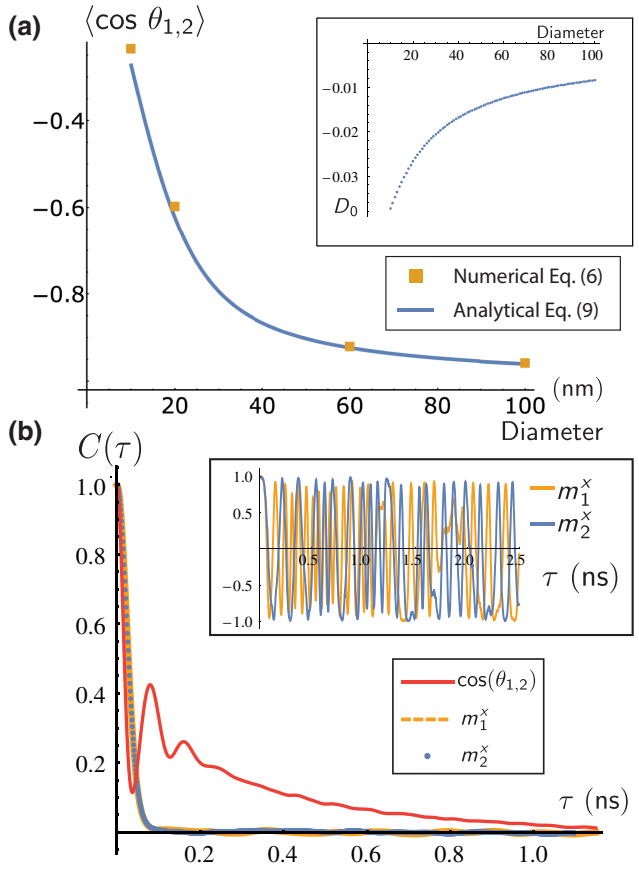

FIG. 4. The zero-bias behavior. (a) The average $\cos\theta_{1,2}$ ($\theta_{1,2}$ is the angle between magnetizations vectors) at zero bias. Equation (9) is compared with a finite-temperature LLG simulation at different diameters (measured in nanometers). The average is taken over 5 μs for all examples with a time step of $\Delta t = 1$ ps. The inset shows the average dipolar tensor component $D_{xx} = D_{yy} = D_0$ as a function of the diameter, calculated from Eq. (4) assuming the same geometric and magnetic parameters that are used in Fig. 2 and damping coefficient $\alpha = 0.01$. (b) The normalized autocorrelation of m^x for both layers and $\cos(\theta_{1,2})$ are shown for $2R = 10$ nm as an example, where the total simulation period is 5 μs. The inset shows the time dependence of the m^x components for a short period.

remain in the x-y plane in equilibrium. Expressing this assumption mathematically, we expand the integrand in Eq. (8) at $(\theta, \eta) \to (\pi/2, \pi/2)$ and keeping the leading order terms, we obtain

$$\langle \cos\theta_{1,2} \rangle \approx \frac{I_1(d_0)}{I_0(d_0)}, \tag{9}$$

where I_n is the modified Bessel function of the first kind.

This simple expression determines the degree of coupling between the two layers in terms of the cosine of the angle between their magnetization and is entirely dependent on geometric and material parameters. Figure 4(a) shows a comparison of Eq. (9) with numerical simulation of Eq. (6) and we observe that the analytical expression reproduces the numerically observed average with high accuracy, especially at higher diameters, where our assumption of $h_d \gg 1$ becomes more accurate. The slight deviation at low diameters $(10, 20)$ nm is due to this assumption becoming inaccurate. Equation (9) is an important result of this paper since, as we see in Sec. V, the average angle behaves in a bias-independent manner; therefore, Eq. (9) is also approximately valid in the nonequilibrium condition. By providing the average degree of coupling between the layers in terms of material and geometric parameters, Eq. (9) could be useful in the design process of double-free-layer MTJs.

We observe from Fig. 4(a) (inset) that even though the average dipolar interaction strength D_0 decreases at high diameters, the coupling strength observed through the average angle between the magnetizations increases [Fig. 4(a)]. The reason for this is that increasing the diameter increases the volume and the dipolar coupling energy as $\propto R^2$ compared to the thermal energy $k_B T$, while the dipolar interaction scales as $\propto R^{-1}$. In other words, the decrease in the dipolar coupling at high diameters is not enough to compensate for the rapidly increasing dipolar energy.

Another interesting observation is made when we observe the autocorrelation,

$$C(\tau) = \frac{1}{T_p} \int m^x(t) m^x(t+\tau) dt, \tag{10}$$

of two in-plane components m^x [Fig. 4(b)], where T_p is the simulation period. The m^x components of each layer lose memory very rapidly in around 100 ps but the cosine of the angle between the magnets takes about 1 ns to become completely uncorrelated. Since this is the parameter that determines the resistance of the MTJ, it is the more relevant time scale to consider to generate random signals. Note that in our analysis, we do not include the effects of exchange interaction between the layers that might be present in real MTJs, as we assume that MgO produces a low degree of exchange coupling compared to the dipolar coupling [55], but this may require further investigation. We also ignore the effect of an existing interfacial anisotropy in our energy model. The existence of a strong interfacial anisotropy may be detrimental to the speed of fluctuations [26]; hence strategies to reduce it might be useful.

V. VOLTAGE-DEPENDENT BEHAVIOR

In order to describe the full bias dependence of the double-free-layer MTJ, we first introduce our combined transport and magnetization dynamics model (Fig. 3). We describe the MTJ as a bias-dependent resistor that provides a bias-dependent spin-polarized current to two separate

finite-temperature LLG solvers described by Eq. (6). The LLG solvers provide magnetization vectors that change the resistance of the MTJ. This self-consistency between the resistance that depends on magnetization and magnetization that depends on resistance is well defined since magnetization dynamics are far slower than the electronic time scales; as such, at each time point, the resistance of the MTJ can be taken as a lumped model that provides spin-polarized currents to the LLG solvers. Similarly, the dipolar coupling acts "instantaneously," providing updated fields that are fed back into the LLG solver at each time step.

We model the bias-dependent conductance ($G_{\rm MTJ} \equiv 1/R_{\rm MTJ}$) based on two voltage-dependent interface polarizations [53,57,58]:

$$G_{\rm MTJ}(V) = G_0\left[1 + P_1(V)P_2(V)\cos\theta_{1,2}\right], \tag{11}$$

where V is the bias voltage across the MTJ, G_0 is the conductance measured when $\cos\theta_{1,2} = \pi/2$, and the $P_i(V)$ are the voltage-dependent polarizations of the two interfaces. By a physically motivated choice of interface polarizations, this model reproduces the bias dependence of the resistance, as well as the asymmetric bias dependence of the spin-polarized current, $\vec{I}_S(V)$ [57]. A reasonable model for the polarization is [53]

$$P(V) = \frac{1}{1 + P_0\exp(-V/V_0)}, \tag{12}$$

where P_0 is a parameter that is determined by the low-bias magnetoresistance and V_0 is determined by the high-bias features of the MTJ. This model is motivated by the observation that at higher voltages, the polarization of the injected currents becomes weaker considering parabolic ferromagnetic bands in the contacts [57].

For simplicity, we assume a symmetric junction where $P_1(V) = P_2(-V) = P(V)$ is satisfied and we drop the subscript to denote only one polarization function, defined by Eq. (12). We also assume a weak dependence of the polarization with respect to the voltage by choosing a large roll-off parameter (V_0) compared to the applied biases of interest (approximately ± 0.5 V) for the p-bit considered in Sec. VI. In actual experiments, the bias dependence of the torque can be controlled by the roll-off parameter that can introduce asymmetries in larger biases depending on the bias asymmetry of the spin-polarized currents, similar to what is observed in standard MTJs [57].

With the bias-dependent polarizations and conductance of the MTJ defined, we can define the magnetization-dependent spin-polarized current in the channel as [57,59]

$$\vec{I}_S(V) = G_0 V[P(V)\hat{m}_1 + P(-V)\hat{m}_2], \tag{13}$$

where the total spin-polarized current is the vectorial sum of two components proportional to the magnetization of each layer. In typical descriptions of spin-transfer-torque in MTJs, only one of these terms appear since the fixed layer is assumed to be inert. In the double-free-layer system, however, both magnets are active and they respond to spin-polarized currents that are polarized in the direction of the other magnets; therefore, we need to consider the total spin-polarized current. A key point to note is that Eq. (13) describes the total spin-polarized current in the channel. For one free layer, $+\vec{I}_s$ is incident to the ferromagnetic interface and for the other layer $-\vec{I}_s$ is incident to the interface. Therefore, what is supplied to the LLG equations differs by a minus sign (Fig. 3). This can also be intuitively understood by considering one free layer as the instantaneously fixed reference layer of the other one: A $+V$ ($-V$) bias that would make the layers parallel (antiparallel) would switch sign if we imagine the other magnet as the reference layer.

There is also another term that is along a direction that is orthogonal to both $\hat{m}_1$ and $\hat{m}_2$, the so-called fieldlike torque, but it is typically small compared to the main terms and we ignore it in this paper [60–62]. The form of Eq. (13) can be justified by microscopic quantum transport models based on the nonequilibrium Green's function (NEGF) formalism that is able to reproduce the bias dependence of torque and resistance values in experiments [57]. Even though there are two terms in Eq. (13), the individual magnetization dynamics of each free layer only pick up a torque from the transverse component of the other free layer [63], since the form of Eq. (6) ensures that $\hat{m}_i \times \vec{I}_S \times \hat{m}_i$ cancels out components of $\vec{I}_S$ along $\hat{m}_i$. We put together all the ingredients discussed so far, the dipolar tensors based on Eq. (4), the finite-temperature LLG dynamics based on Eq. (6), and the transport equations of MTJ described by Eqs. (11)–(13), in a modular circuit environment [53] that is simulated in HSPICE (Fig. 3).

Figure 5 shows representative voltage-dependent characteristics of a double-free-layer MTJ. A striking finding is that the bias dependence of the resistance is approximately independent of the applied voltage, even in the presence of the full effect of spin-transfer-torque between the layers. The bias dependence also shows symmetry with respect to voltage, a result we intuitively expect since the device is completely symmetric with two identical free layers. Figure 5(a) illustrates the dynamics of the free layers at different time instances. We observe that the free layers fluctuate close to the x-y plane but also occasionally pick up a z component. These fluctuations are reminiscent of the fast precessional fluctuations of easy-plane magnets that have been examined in Refs. [20,26,27] but all with stable reference layers, unlike the case considered here.

Figure 5(b) shows the R versus V characteristics of a 10-nm double-free-layer MTJ where the resistance keeps fluctuating approximately uniformly between $R_{\rm P}$ and $R_{\rm AP}$ values at all bias voltages. This bias independence of the

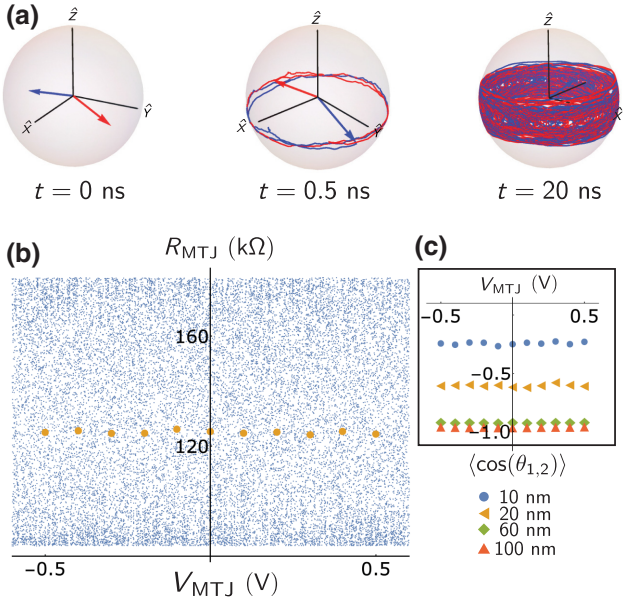

FIG. 5. The R versus V characteristics of a double-free-layer MTJ. (a) Representative fluctuations at different time instances for $2R = 20$ nm free layers at $t = 0$ ns, $t = 0.5$ ns, and $t = 20$ ns. (b) The R versus V characteristics for a $(2R) = 10$ nm MTJ, where we assume a low-bias TMR of 115% [$P_0 = 0.65$ and $V = 0$ in Eq. (12)] and a roll-off constant $V_0 = 50$ V, ensuring a symmetric bias dependence for the spin-polarized currents. We assume an RA product of 9Ω-μm^2 [56] to obtain G_0 for all MTJs in this paper. The plot is obtained by sweeping the voltage from $(-2$ V, 2 V) in 2 μs with 1-ps time steps; the dots correspond to 1-μs averages taken at that bias. (c) The average $\cos(\theta_{1,2})$ taken over 1 μs at different bias points for different diameters. All diameters roughly show bias-independent average angles or resistances.

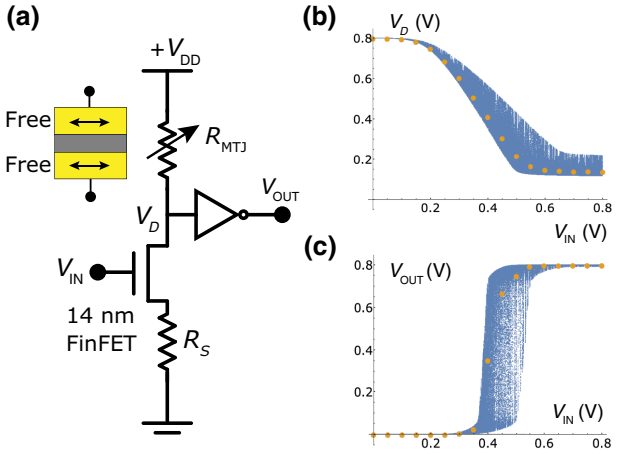

FIG. 6. A BSN with a double-free-layer MTJ. (a) The double-free-layer MTJ ($2R = 20$ nm with all the same parameters that are used in previous figures) in a 1T-1MTJ circuit, where a $R_S = 5k\Omega$ resistance is used to shift the overall characteristics. (b) The drain voltage is measured while the input is swept from 0 V to 0.8 V over 0.5 μs. The circled points are averages over 250 ns at each bias point. (c) The output of the inverter, which shows the BSN characteristics with the same measurement times as reported in (b).

fluctuations is a significant advantage of the double-free-layer MTJ, since it can provide a fluctuating resistance over a wide range of values without getting pinned, unlike MTJs with fixed layers [14,20], where the random fluctuation point needs to be identified carefully in an eventual device implementation. We also note from Fig. 5(c) that above 60–100 nm, the average of the angle (and the resistance of the MTJ), even though random, is largely stuck around the R_{AP} value where the increasing dipolar energy with magnetic volume overcomes the thermal noise. For this reason, strategies to use scaled dimensions or low-magnetic-moment (M_s) materials will be useful.

VI. TUNABLE RANDOMNESS WITH DOUBLE-FREE-LAYER MTJ

In this section, we show how the double-free-layer MTJ can be used to deliver a hardware binary-stochastic-neuron (BSN) functionality in a 1T-1MTJ circuit plus an inverter circuit (Fig. 6) based on Ref. [22], although we attach a source resistance R_S to be able to shift the overall characteristics to the left or to the right, similar to what has been carried out in Ref. [14]. We use a high-performance 14-nm FinFET model from the PREDICTIVE TECHNOLOGY MODEL (PTM) [64] to model the NMOS and combine the NMOS model with our circuit model simulated in HSPICE. We choose the 20-nm MTJ (with the same parameters that are used in this paper) to illustrate the circuit operation (Fig. 6), since its average resistance ($1/G_0$) approximately matches the transistor resistance plus the source resistance (R_S) when the input to the NMOS is 0.4 V. Our purpose is not to provide a comprehensive circuit design of the BSN but simply to illustrate how the proposed MTJ, which includes effects of thermal noise, dipolar coupling, and bias-dependent spin and charge currents, can be used to build a viable hardware BSN.

Figure 6 shows the output of the inverter while the input gate voltage of the NMOS is swept from 0 to V_{DD}, the average of which shows the familiar sigmoidal behavior of the binary stochastic neuron (BSN). One potential challenge in the design of double-free-layer MTJs will undoubtedly be to design the average P/AP ratio of the fluctuations. Indeed, as can be observed from Fig. 5(c), the average resistance of the MTJ at different diameters is not in the middle of R_P and R_{AP} values but closer to R_{AP} due to the dipolar coupling of the in-plane free layers. While at very high diameters > 60 nm, this ratio may mostly be skewed toward R_{AP}, the skew at 20 nm can be mitigated by a source resistance (R_S) to center the sigmoid of the hardware BSN, as shown in Fig. 6. We observe that changing this resistance value causes a shift of the overall characteristics (with higher values causing a rightward shift).

Unlike previous stochastic MTJs in which the bias point where fluctuations between R_{AP} and R_P can vary significantly between different devices, the weak bias dependence of the proposed MTJ can be globally centered by a fixed source resistance. This difference between having to align each p-bit precisely at its midpoint by a different bias current and obtaining an approximately uniform randomness at all relevant bias voltages constitutes an important advantage of the proposed design that can be exploited at the system level. Secondary variations arising from differences in MTJ resistances and transistor process variations can further be dealt with at the "synaptic level," where weighted inputs of p-bits can be modified by constant biases to counter these variations. Further, probabilistic computations are generally robust to small variations [65,66] and strategies that may counter such variations by adjusting the interconnection weights of probabilistic devices (as has been done in Ref. [14]) can be useful.

Moreover, ultrascaled MTJs beyond 20 nm can become truly random as predicted by Eq. (9) provided that we can match the resistance of the NMOS to that of the MTJ, either by transistor design or by an additional source resistance, as shown in Fig. 6. Device-level simulations have shown that BSN characteristics similar to those shown in Fig. 6 can be used as building blocks to design probabilistic circuits to solve optimization [22,67,68] and sampling problems to train neural networks [69]. Therefore, the proposed double-free-layer MTJ can function in similar ways to be useful for these applications.

It is important to note that even though we present the double-free-layer MTJ in terms of circular-disk magnets that can fluctuate in nanosecond time scales, recent experimental [20,29] and theoretical work [26–28] have now firmly established that elliptical in-plane easy-axis magnets can also fluctuate in similar time scales. While the exact details of our model might be different, the double-free-layer concept as a bias-dependent building block to build probabilistic bits applies to such structures with qualitatively similar results.

VII. CONCLUSION

We propose and analyze a MTJ with two free layers to generate random fluctuations using a comprehensive model where the dipolar interaction, thermal noise, and bias-dependent spin and charge currents are considered. Our findings reveal approximately bias-independent magnetization fluctuations that can produce random resistance values over a wide range of bias values, which can simplify circuit design with such MTJs. Another key advantage of the proposed magnetic stack is in its simplicity: the two free layers can be completely symmetric and their in-plane magnetization can easily be achieved by modifying the existing STT MRAM technology by increasing the thickness of both the free and the fixed layers. Repurposing STT MRAM technology with double-free-layer MTJs can lead to massively parallel tunable random number generators that can find useful applications in probabilistic computing.

ACKNOWLEDGMENTS

Use was made of computational facilities purchased with funds from the National Science Foundation (Grant No. CNS-1725797) and administered by the Center for Scientific Computing (CSC). The CSC is supported by the California NanoSystems Institute and the Materials Research Science and Engineering Center (MRSEC; NSF DMR 1720256) at University of California Santa Barbara. K.Y.C. and M.M.T. thank Daryl Lee from the Department of Electrical and Computer Engineering at University of California Santa Barbara for providing computational resources during the course of this project. K.Y.C. gratefully acknowledges fruitful discussions with Jan Kaiser, Orchi Hassan, and Supriyo Datta. The work is partly supported by Japan Science and Technology Agency (JST) CREST project JPMJCR19K3.

[1] A. Parihar, N. Shukla, M. Jerry, S. Datta, and A. Raychowdhury, Computing with dynamical systems based on insulator-metal-transition oscillators, Nanophotonics **6**, 601 (2017).

[2] N. Locatelli, V. Cros, and J. Grollier, Spin-torque building blocks, Nat. Mater. **13**, 11 (2014).

[3] A. Fukushima, T. Seki, K. Yakushiji, H. Kubota, H. Imamura, S. Yuasa, and K. Ando, Spin dice: A scalable truly random number generator based on spintronics, Appl. Phys. Exp. **7**, 083001 (2014).

[4] W. H. Choi, Y. Lv, J. Kim, A. Deshpande, G. Kang, J.-P. Wang, and C. H. Kim, in *Electron Devices Meeting (IEDM), 2014 IEEE International* (IEEE, San Fransisco, CA, USA, 2014), p. 12.

[5] Y. Kim, X. Fong, and K. Roy, Spin-orbit-torque-based spin-dice: A true random-number generator, IEEE Magn. Lett. **6**, 1 (2015).

[6] H. Lee, F. Ebrahimi, P. K. Amiri, and K. L. Wang, Design of high-throughput and low-power true random number generator utilizing perpendicularly magnetized voltage-controlled magnetic tunnel junction, AIP Adv. **7**, 055934 (2017).

[7] B. Parks, M. Bapna, J. Igbokwe, H. Almasi, W. Wang, and S. A. Majetich, Superparamagnetic perpendicular magnetic tunnel junctions for true random number generators, AIP Adv. **8**, 055903 (2018).

[8] D. Vodenicarevic, N. Locatelli, A. Mizrahi, J. S. Friedman, A. F. Vincent, M. Romera, A. Fukushima, K. Yakushiji, H. Kubota, S. Yuasa, S. Tiwari, J. Grollier, and D. Querlioz, Low-Energy Truly Random Number Generation with Superparamagnetic Tunnel Junctions for Unconventional Computing, Phys. Rev. Appl. **8**, 054045 (2017).

[9] D. Vodenicarevic, N. Locatelli, A. Mizrahi, T. Hirtzlin, J. S. Friedman, J. Grollier, and D. Querlioz, in *2018 IEEE International Symposium on Circuits and Systems (ISCAS)* (IEEE, Florence, Italy, 2018), p. 1.

[10] Y. Lv and J.-P. Wang, in *Electron Devices Meeting (IEDM), 2017 IEEE International* (IEEE, San Fransisco, CA, USA, 2017), p. 36.

[11] C. M. Liyanagedera, A. Sengupta, A. Jaiswal, and K. Roy, Stochastic Spiking Neural Networks Enabled by Magnetic Tunnel Junctions: From Nontelegraphic to Telegraphic Switching Regimes, Phys. Rev. Appl. **8**, 064017 (2017).

[12] P. Debashis and Z. Chen, in *2018 76th Device Research Conference (DRC)* (IEEE, Santa Barbara, CA, USA, 2018), p. 1.

[13] A. Mizrahi, T. Hirtzlin, A. Fukushima, H. Kubota, S. Yuasa, J. Grollier, and D. Querlioz, Neural-like computing with populations of superparamagnetic basis functions, Nat. Commun. **9**, 1533 (2018).

[14] W. A. Borders, A. Z. Pervaiz, S. Fukami, K. Y. Camsari, H. Ohno, and S. Datta, Integer factorization using stochastic magnetic tunnel junctions, Nature **573**, 390 (2019).

[15] V. Ostwal and J. Appenzeller, Spin-orbit torque-controlled magnetic tunnel junction with low thermal stability for tunable random number generation, IEEE Magn. Lett. **10**, 1 (2019).

[16] M. Ahsanul Abeed and S. Bandyopadhyay, Low barrier nanomagnet design for binary stochastic neurons: Design challenges for real nanomagnets with fabrication defects, IEEE Magn. Lett. **10**, 1 (2019).

[17] M. W. Daniels, A. Madhavan, P. Talatchian, A. Mizrahi, and M. D. Stiles, Energy-Efficient Stochastic Computing with Superparamagnetic Tunnel Junctions, Phys. Rev. Appl. **13**, 034016 (2020).

[18] B. Parks, A. Abdelgawad, T. Wong, R. F. L. Evans, and S. A. Majetich, Magnetoresistance Dynamics in Superparamagnetic Co-Fe-B Nanodots, Phys. Rev. Appl. **13**, 014063 (2020).

[19] S. Ganguly and A. W. Ghosh, in *International Conference on Neuromorphic Systems 2020* (ACM, Oak Ridge, TN, USA, 2020), p. 1.

[20] C. Safranski, J. Kaiser, P. Trouilloud, P. Hashemi, G. Hu, and J. Z. Sun, Nano Lett. **21**, 2040 (2021).

[21] J. Cai, B. Fang, L. Zhang, W. Lv, B. Zhang, T. Zhou, G. Finocchio, and Z. Zeng, Voltage-Controlled Spintronic Stochastic Neuron Based on a Magnetic Tunnel Junction, Phys. Rev. Appl. **11**, 034015 (2019).

[22] K. Y. Camsari, S. Salahuddin, and S. Datta, Implementing p-bits with embedded MTJ, IEEE Electron Device Lett. **38**, 1767 (2017).

[23] K. Y. Camsari, B. M. Sutton, and S. Datta, p-bits for probabilistic spin logic, Appl. Phys. Rev. **6**, 011305 (2019).

[24] W. T. Coffey and Y. P. Kalmykov, Thermal fluctuations of magnetic nanoparticles: Fifty years after Brown, J. Appl. Phys. **112**, 121301 (2012).

[25] K. Y. Camsari, R. Faria, B. M. Sutton, and S. Datta, Stochastic p-Bits for Invertible Logic, Phys. Rev. X **7**, 031014 (2017).

[26] J. Kaiser, A. Rustagi, K. Y. Camsari, J. Z. Sun, S. Datta, and P. Upadhyaya, Subnanosecond Fluctuations in Low-Barrier Nanomagnets, Phys. Rev. Appl. **12**, 054056 (2019).

[27] O. Hassan, R. Faria, K. Y. Camsari, J. Z. Sun, and S. Datta, Low-barrier magnet design for efficient hardware binary stochastic neurons, IEEE Magn. Lett. **10**, 1 (2019).

[28] S. Kanai, K. Hayakawa, H. Ohno, and S. Fukami, Theory for relaxation time of stochastic nanomagnets, Phys. Rev. B **103**, 094423 (2021).

[29] K. Hayakawa, S. Kanai, T. Funatsu, I. J. Jinnai B., W. A. Borders, H. Ohno, and S. Fukami, Nanosecond Random Telegraph Noise in In-Plane Magnetic Tunnel Junctions, Phys. Rev. Lett. **126**, 117202 (2021).

[30] S. Bhatti, R. Sbiaa, A. Hirohata, H. Ohno, S. Fukami, and S. N. Piramanayagam, Spintronics based random access memory: A review, Mater. Today **20**, 530 (2017).

[31] K. Kudo, R. Sato, and K. Mizushima, Synchronized magnetization oscillations in F/N/F nanopillars, Jpn. J. Appl. Phys. **45**, 3869 (2006).

[32] G. E. Rowlands and I. N. Krivorotov, Magnetization dynamics in a dual free-layer spin-torque nano-oscillator, Phys. Rev. B **86**, 094425 (2012).

[33] T. Taniguchi, Synchronized, periodic, and chaotic dynamics in spin torque oscillator with two free layers, J. Magn. Magn. Mater. **483**, 281 (2019).

[34] R. Matsumoto, S. Lequeux, H. Imamura, and J. Grollier, Chaos and Relaxation Oscillations in Spin-Torque Windmill Spiking Oscillators, Phys. Rev. Appl. **11**, 044093 (2019).

[35] W. Zhou, H. Sepehri-Amin, T. Taniguchi, S. Tamaru, Y. Sakuraba, S. Kasai, H. Kubota, and K. Hono, Inducing out-of-plane precession of magnetization for microwave-assisted magnetic recording with an oscillating polarizer in a spin-torque oscillator, Appl. Phys. Lett. **114**, 172403 (2019).

[36] I. D. Mayergoyz, G. Bertotti, and C. Serpico, *Nonlinear Magnetization Dynamics in Nanosystems* (Elsevier, Oxford, UK, 2009).

[37] G. B. Arfken and H. J. Weber, *Mathematical Methods for Physicists* (Harcourt Brace Jovanovich, San Diego, Academic Press, 1967).

[38] E. M. Purcell, *Electricity and Magnetism*, type Tech. Rep. (1965).

[39] T. Taniguchi, An analytical computation of magnetic field generated from a cylinder ferromagnet, J. Magn. Magn. Mater. **452**, 464 (2018).

[40] M. Gajek, J. J. Nowak, J. Z. Sun, P. L. Trouilloud, E. J. O'sullivan, D. W. Abraham, M. C. Gaidis, G. Hu, S. Brown, Y. Zhu, *et al.*, Spin torque switching of 20 nm magnetic tunnel junctions with perpendicular anisotropy, Appl. Phys. Lett. **100**, 132408 (2012).

[41] A. J. Newell, W. Williams, and D. J. Dunlop, A generalization of the demagnetizing tensor for nonuniform magnetization, J. Geophys. Res.: Solid Earth **98**, 9551 (1993).

[42] G. M. Wysin, *Magnetic Excitations and Geometric Confinement* (IOP, Philadelphia, USA, 2015).

[43] W. H. Butler, T. Mewes, C. K. A. Mewes, P. B. Visscher, W. H. Rippard, S. E. Russek, and R. Heindl, Switching distributions for perpendicular spin-torque devices within the macrospin approximation, IEEE Trans. Magn. **48**, 4684 (2012).

[44] J. Z. Sun, Spin-current interaction with a monodomain magnetic body: A model study, Phys. Rev. B **62**, 570 (2000).
[45] J. Z. Sun, T. S. Kuan, J. A. Katine, and R. H. Koch, in *Quantum Sensing and Nanophotonic Devices*, Vol. 5359 (International Society for Optics and Photonics, San Jose, CA, USA, 2004), p. 445.
[46] T. Shinjo, T. Okuno, R. Hassdorf, K. Shigeto, and T. Ono, Magnetic vortex core observation in circular dots of permalloy, Science **289**, 930 (2000).
[47] C. D. Moreira, M. G. Monteiro Jr, D. Toscano, S. A. Leonel, and F. Sato, Decreasing the size limit for a stable magnetic vortex in modified permalloy nanodiscs, J. Magn. Magn. Mater. **443**, 252 (2017).
[48] M.-F. Lai and C.-N. Liao, Size dependence of *C* and *S* states in circular and square permalloy dots, J. Appl. Phys. **103**, 07E737 (2008).
[49] J. K. Ha, R. Hertel, and J. Kirschner, Micromagnetic study of magnetic configurations in submicron permalloy disks, Phys. Rev. B **67**, 224432 (2003).
[50] R. P. Cowburn, D. K. Koltsov, A. O. Adeyeye, M. E. Welland, and D. M. Tricker, Single-Domain Circular Nanomagnets, Phys. Rev. Lett. **83**, 1042 (1999).
[51] P. Debashis, R. Faria, K. Y. Camsari, J. Appenzeller, S. Datta, and Z. Chen, in *2016 IEEE International Electron Devices Meeting (IEDM)* (IEEE, San Fransico, CA, USA, 2016), p. 34.
[52] P. Debashis, R. Faria, K. Y. Camsari, and Z. Chen, Design of stochastic nanomagnets for probabilistic spin logic, IEEE Magn. Lett. **9**, 1 (2018).
[53] M. M. Torunbalci, P. Upadhyaya, S. A. Bhave, and K. Y. Camsari, Modular compact modeling of MTJ devices, IEEE Trans. Electron Devices **65**, 4628 (2018).
[54] B. Behin-Aein, D. Datta, S. Salahuddin, and S. Datta, Proposal for an all-spin logic device with built-in memory, Nat. Nanotechnol. **5**, 266 (2010).
[55] H. X. Yang, M. Chshiev, A. Kalitsov, A. Schuhl, and W. H. Butler, Effect of structural relaxation and oxidation conditions on interlayer exchange coupling in Fe—MgO—Fe tunnel junctions, Appl. Phys. Lett. **96**, 262509 (2010).
[56] C. J. Lin, S. H. Kang, Y. J. Wang, K. Lee, X. Zhu, W. C. Chen, X. Li, W. N. Hsu, Y. C. Kao, M. T. Liu, *et al.*, in *Electron Devices Meeting (IEDM), 2009 IEEE International* (IEEE, Baltimore, MD, USA, 2009), p. 1.
[57] D. Datta, B. Behin-Aein, S. Datta, and S. Salahuddin, Voltage asymmetry of spin-transfer torques, IEEE Trans. Nanotechnol. **11**, 261 (2011).
[58] D. Datta, Ph.D. thesis, School of Electrical and Computer Engineering, Purdue University (2012).
[59] K. Y. Camsari, S. Ganguly, D. Datta, and S. Datta, in *Electron Devices Meeting (IEDM), 2014 IEEE International* (IEEE, San Fransico, CA, USA, 2014), p. 35.
[60] H. Kubota, A. Fukushima, K. Yakushiji, T. Nagahama, S. Yuasa, K. Ando, H. Maehara, Y. Nagamine, K. Tsunekawa, D. D. Djayaprawira, *et al.*, Quantitative measurement of voltage dependence of spin-transfer torque in MgO-based magnetic tunnel junctions, Nat. Phys. **4**, 37 (2008).
[61] C. Wang, Y.-T. Cui, J. A. Katine, R. A. Buhrman, and D. C. Ralph, Time-resolved measurement of spin-transfer-driven ferromagnetic resonance and spin torque in magnetic tunnel junctions, Nat. Phys. **7**, 496 (2011).
[62] S. Boyn, J. Sampaio, V. Cros, J. Grollier, A. Fukushima, H. Kubota, K. Yakushiji, and S. Yuasa, Twist in the bias dependence of spin torques in magnetic tunnel junctions, Phys. Rev. B **93**, 224427 (2016).
[63] M. D. Stiles and A. Zangwill, Anatomy of spin-transfer torque, Phys. Rev. B **66**, 014407 (2002).
[64] PREDICTIVE TECHNOLOGY MODEL (PTM) (http://ptm.asu.edu/).
[65] A. Zeeshan Pervaiz, L. Anirudh Ghantasala, K. Y. Camsari, and S. Datta, Hardware emulation of stochastic *p*-bits for invertible logic, Sci. Rep. **7**, 10994 (2017).
[66] J. L. Drobitch and S. Bandyopadhyay, Reliability and scalability of *p*-bits implemented with low energy barrier nanomagnets, IEEE Magn. Lett. **10**, 4510404 (2019).
[67] B. Sutton, K. Y. Camsari, B. Behin-Aein, and S. Datta, Intrinsic optimization using stochastic nanomagnets, Sci. Rep. **7**, 44370 (2017).
[68] O. Hassan, K. Y. Camsari, and S. Datta, Voltage-driven building block for hardware belief networks, IEEE Design & Test **36**, 15 (2019).
[69] J. Kaiser, R. Faria, K. Y. Camsari, and S. Datta, Probabilistic circuits for autonomous learning: A simulation study, Front. Comput. Neurosci. **14** (2020).